JET-P(94)64

Modelling of Sawtooth Induced Redistribution of ICRF Heated Minority Ions

D Anderson[1], L-G Eriksson, M Lisak[1], A Ödblom[1].

JET Joint Undertaking, Abingdon, Oxfordshire, OX14 3EA, UK.
[1] Institute for Electromagnetic Field Theory, Chalmers University of Technology, S-412 96 Göteborg, Sweden.

Preprint of a paper to be submitted for publication in Plasma Physics and Controlled Fusion

December 1994

A qualitative model is given to describe the redistribution of ICRF-heated minority ions at sawtooth crashes in Tokamak plasmas. A crucial feature of the model is that it takes into account profile broadening effects due to the finite width of the ICRF-heated particle orbits. Predictions of the model are compared and found to be in agreement with numerical simulations as well as with experimental results from JET.

I. INTRODUCTION

Experimental evidence from JET indicates that sawtooth crashes tend to redistribute ICRF-heated particles [1, 2]. In particular, the rapid reduction of the fast ion energy content following a sawtooth crash, as observed on JET, has been interpreted as an enhanced slowing down of fast ions that have been expelled from the central hot parts to the cooler plasma outside the $q = 1$ surface, [1]. Similarly, a redistribution of fast RF-heated ions has also been inferred from the observed reheating rate of the central electron temperature after sawtooth crashes, [2].

The purpose of the present work is to apply a recently given model for sawtooth-induced fast ion redistribution to the case of ICRF-heated minority ions. However, before such an application can be made, a way must be found to acount for the fact that for high absorbed power densities, most of the RF-heated ions have orbits which deviate strongly from the magnetic surfaces. In section II we present a convenient approach to this problem. The analysis is based on a simplified model which replaces the usually very peaked RF power absorption profiles with a suitably broadened profile which takes into account the smearing out of the RF power due to finite orbit effects. The increased broadening is determined by a suitably chosen average of the orbit width of the RF-heated ions. A comparison with computer simulation results, justifying the simplified approach is also given. To test the model for finite orbit width broadening further, the model is also used, in section III, to analyze the saturation of fast ion energy content with increasing RF-power as observed on JET, [3, 1]. Again the agreement between analytical predictions and numerical simulations / experimental results is found to be good.

Thus, having established the credibility of the orbit broadening model we proceed to analyze, in section IV, the sawteeth - induced redistribution of ICRF-heated minority ions. In agreement with experiments and numerical simulations it is found that the fast ion energy within the central core decreases by typically 40-60 % at a sawtooth crash. Finally, in section V, a qualitative discussion is given of the rapid drop of the total fast ion energy which occurs when fast minority ions, having been expelled from the hot central core by the sawtooth crash, rapidly slow down in the outer colder parts of the plasma.

II. SIMPLE MODEL FOR FINITE ORBIT WIDTH EFFECTS ON FAST ION ENERGY DENSITY PROFILE

The Fokker-Planck equation, including the RF-diffusion operator due to the ICRF heating, can be multiplied by the ion energy and integrated over velocity space to yield the following equation for the fast ion energy density, w (assuming the fast ions to slow down primarily on the electrons)

$$\frac{\partial w}{\partial t} = p - \frac{2}{t_s} w \tag{1}$$

In eq. (1), p is the absorbed RF-power density, t_s is the slowing down time, and w is given by

$$w \equiv \int \frac{1}{2} m v^2 f d^3 v \tag{2}$$

where f is the distribution function of the heated ions and m and v are the mass and velocity respectively of the particle. When the RF-power is turned on, the wave power is spent in establishing the high energy tail distribution of the absorbing ions. However, in steady-state conditions, the absorbed RF-power is mainly transferred from the heated ions to the background plasma electrons by collisions. Due to the finite orbit width of the RF-heated particles, the profile of the collisionally deposited electron heating is broader than the absorbed RF-power profile. To model the broadened electron heating profile, we will replace the actual power deposition profile, p , in eq. (1), with an equivalent profile, $\tilde{p}$ having the same total power but a larger width.

A suitable choice for the width of the broadened power deposition profile can be obtained as follows. Strong ICRF heating creates an almost perpendicular velocity tail of high energy trapped particles with turning points in the resonant layer. For on-axis heating, these particles trace out potato-shaped rather than banana-shaped orbits, cf [4]. The width of a potato orbit, Δ_p, is given by

$$\Delta_p \cong R\Delta^{\frac{2}{3}} \tag{3}$$

where R is the major radius and

$$\Delta = \frac{2q(0)v}{\omega_c R} \tag{4}$$

In eq. (4), q(0) denotes the value of the safety factor on axis, v is the particle velocity, and ω_c is the ion cyclotron frequency. Thus, the half width of the potato orbit normalized to the plasma minor radius, a, can be written

$$\delta \equiv \frac{1}{2}\frac{\Delta_p}{a} = \left(\frac{A}{2}\right)^{\frac{1}{3}} (q(0)\rho_L)^{\frac{2}{3}} \tag{5}$$

where A is the aspect ratio and ρ_L is the normalized Larmor radius of the particle.

We now define a width, δ_{eff}, characterizing the broadening of the power deposition as

$$\delta_{eff} \equiv << \delta(r,v) >> \tag{6}$$

where << >> denotes a weighted average over velocity space and geometrical space according to

$$\begin{aligned} <\delta> &\equiv \frac{\int \frac{1}{2} m v^2 \delta f \, d^3v}{\int \frac{1}{2} m v^2 f \, d^3v} \\ <\delta> &\equiv \frac{\int p(r) <\delta> d^3r}{\int p(r) d^3r} \end{aligned} \tag{7}$$

For minority ICRF-heating the distribution function at the resonance can be approximated as

$$f(v) \sim \exp\left(-\frac{m v_\perp^2}{2T_\perp}\right) \tag{8}$$

where $v_{||}$ and $v_\perp$ are the parallell and perpendicular velocity components and $T_\perp = T_\perp(r)$ is the temperture of the high energy tail. Performing the velocity integrations in eq. (7) we obtain

$$<\delta> \cong 1.2\delta(v_t) \tag{9}$$

where v_t is the tail velocity corresponding to the tail temperature, $T_\perp$, i.e. $\frac{1}{2} m v_t^2 = T_\perp$.

Modelling the power absorption profile, p(r), as

$$p(r) = p(0) e^{-\frac{x^2}{b^2}} \tag{10}$$

where x denotes radius normalized to minor radius, we obtain

$$\delta_{eff} \cong 0.7 A^{\frac{1}{3}} (q(0)\rho_L(0))^{\frac{2}{3}} \tag{11}$$

In eq. (11), $\rho_L(0)$ denotes the Larmor radius corresponding to the tail velocity on axis, $v_t(0)$ which is approximately determined by

$$\frac{1}{2}mv_t^2(0) = T_\perp(0) \cong \frac{p(0)t_s(0)}{2n(0)} \tag{12}$$

where $t_s(0)$ and $n(0)$ are the slowing down time and the minority ion density respectively on axis.

The equivalent broadened power deposition profile, $\tilde{p}(r)$, to be used in our subsequent analysis is then taken as

$$\tilde{p}(r) = \tilde{p}(0)e^{-\frac{x^2}{(b+\delta_{eff})^2}} \tag{13}$$

where in order to conserve the total absorbed power

$$\tilde{p}(0) = \frac{p(0)}{(1+\delta_{eff}/b)^2} \tag{14}$$

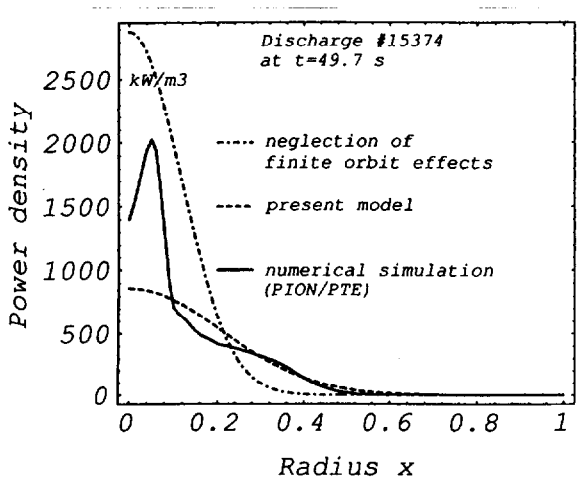

Fig.1. Comparison between collisionally transferred power to the electrons, -·-·- finite orbit effects neglected, --- numerical simulation results including finite orbit effects (PION/PDTE), and --- present simplified model.

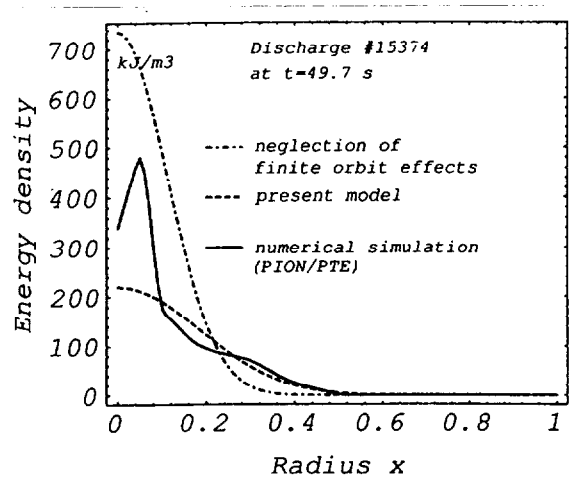

Fig. 2. Comparison between fast ion energy density profiles, -·-·- finite orbit effects neglected, --- numerical simulations including finite orbit effects (PION/WD1), and --- present simplified model.

A more detailed comparison between numerical simulations and the predictions of the simplified model given by eqs. (11-13) will be given elsewhere. However, an example of the agreement is given in Figs.1 and 2 which compare predictions and simulation results for the

electron heating and fast ion energy density profiles for a case of strong RF-heating where finite orbit effects are important.

We note that the over all agreement is very good. The simplified model is unable to reproduce the central peaking feature observed in the numerical simulations. However, since the corresponding volume elements are small the simplified model is expected to yield good accuracy for averaged or integrated quantities.

Finally, we note that a similar model was previously used in [5] except that the present analysis contains a prescription for the proper value of δ_{eff}, cf eq. (11).

III. EFFECT OF FINITE ORBIT WIDTH ON TOTAL FAST ION ENERGY

It has been observed on JET that the increase of the total energy of the RF-heated minority ions tends to saturate at high absorbed RF powers. This was explained in terms of finite orbit effects in Ref. [3]. An alternative and simpler model to account for the saturation can be given based on the model of the previous paragraph.

From eq. (1) we infer that in steady state the fast ion energy density profile, w(x), is determined by

$$w(x) = \frac{1}{2} t_s(x) p(x) \tag{15}$$

Usually the slowing down profile is modelled as a generalized parabola, i.e.

$$t_s(x) = t_s(0)\left(1 - x^2\right)^{\mu} \tag{16}$$

A similar approximation can be given for p(x) using the fact that, if $b^2 << 1$, then to very good accuracy we can write

$$\exp\left(-\frac{x^2}{b^2}\right) \approx \left(1 - x^2\right)^{\nu} \tag{17}$$

where $\nu = 1/b^2 - 1$.

This implies that

$$w(x) = w(0)\left(1 - x^2\right)^{\gamma} \tag{18}$$

where $w(0) = t_s(0)p(0)/2$ and

$$\gamma = \nu + \mu \tag{19}$$

Integrating eq. (1) over space we obtain the following equation for the evolution of the total fast ion energy content, $W = \langle w \rangle$:

$$\frac{dW}{dt} = P - \left\langle \frac{2w}{t_s} \right\rangle \tag{20}$$

where $\langle\ \rangle$ denotes integration over plasma volume in the straight cylinder approximation and $P = \langle p \rangle$.

In steady-state we obtain, using equations (16) and (18),

$$W = \frac{1}{2}\bar{t}_s P \tag{21}$$

where

$$\bar{t}_s = \frac{\nu+1}{\nu+1+\mu} t_s(0) \tag{22}$$

We note that $\bar{t}_s$, given by eq. (22), plays the same role as the "self consistent slowing down time" obtained in [3] by averaging over particle orbit and velocity distribution. Equations (21) and (22) should be useful for estimating the total fast ion energy content in discharges subject to ICRF minority heating.

A detailed comparison between experimental measurements and the results of extensive numerical simulations for ICRF minority heated discharges in JET was recently presented, [1]. This comparison demonstrated that it is necessary to include finite orbit corrections in order to obtain good agreement for high power ICRF heated discharges. The application of the present simplified approach can be illustrated by considering one of the discharges analyzed in [1].

For the discharge (#12298), the total absorbed power was 8.0 MW of which 6 MW was estimated to be absorbed by the minority ions. The on-axis slowing down time was given as $t_s(0) = 0.63$ s, the width of the power deposition profile was $b \approx 0.25$, and the slowing down profile exponent $\mu \cong 4$. Using eq. (21), this implies $W \cong 1.5$ MJ, in good agreement with the simulation results neglecting finite orbit corrections. However, the experimental results indicated a reduced fast ion energy of approximately 1 MJ, which was found to be in good agreement with simulation results when finite orbit corrections were included.

In order to determine the orbit broadening effect we need to estimate the on-axis tail temperature. The centrally absorbed power density is of the order of 1 MW/m^3 , which for a 6% minority hydrogen concentration in a plasma with the electron density, $n_e \cong 3.6 \cdot 10^{19}\ m^{-3}$ implies a tail temperature $T_\perp = 2$ MeV. The corresponding effective orbit width is $\delta_{eff} \approx 0.20$ resulting in a total width for the electron heating of 0.45, in reasonable agreement with the numerical simulation results when finite orbit widths are included. Furthermore, when the

broadened profile is used in eq.s (21) and (22) we obtain W ≅ 1 MJ in agreement with simulation results and experiment.

In addition to the discharge above, the present approach has been applied to two other discharges analyzed in [1] as well as three further pulses. The results are summarized in Table I and show good agreement with experimental results.

Table I

pulse	$t_s(0)$ s	P_{ce} MW	p(0) MW/m^3	$T_\perp$ MeV	b	δ_{eff}	μ	γ_{eff}	Wo MJ	W MJ	W exp MJ
19650	0.63	5.5	0.7	0.8	0.35	0.12	3.1	7	1.3	1.0	1.1
12295	0.60	3.0	0.8	0.8	0.25	0.15	4.0	9	0.7	0.6	0.6
12298	0.63	6.0	1.6	1.4	0.25	0.19	4.0	8	1.5	1.1	1.0
15374	0.51	4.5	2.8	2.1	0.16	0.15	3.7	13	1.0	0.8	0.7
15380	0.37	5.6	2.0	0.8	0.21	0.11	2.5	11	0.9	0.8	0.9
15433	0.36	5.0	0.7	0.6	0.33	0.10	2.6	7	0.7	0.6	0.6

Table I. Effects of finite orbit width on total fast ion energy. A comparison between theoretical predictions and experimental results. The theoretical predictions are based on A = 3.15, q(0) = 1, P_{ce} denotes power transferred to electrons from fast ion slowing down, and γ_{eff} is the profile exponent of the orbit broadened fast ion energy density.

The degrading effect of finite orbit width on total fast ion energy can be further illustrated as follows: using eqs. (21) and (22) we can write

$$\frac{W}{W_o} = \frac{1+\mu b^2}{1+\mu(b+\delta_{eff})^2} \tag{23}$$

where W_0 denotes the total energy in the absence of finite orbit width corrections. Furthermore, using eq. (11) we can rewrite eq. (23) as

$$\frac{W}{W_o} = \frac{1+\mu b^2}{1+\mu b^2\left(1+\left(\frac{T_\perp(0)}{T_*}\right)^{\frac{1}{3}}\right)^2} \tag{24}$$

where the critical temperature, T_* is given by

$$T_* \cong 1.4\cdot 10^2 \frac{b^3}{MA}\left(\frac{Za(m)B(T)}{q(0)}\right)^2 (MeV) \tag{25}$$

In eq. (25) M and Z denote the mass number and the charge number respectively of the heated ions. As an example we note that taking b = 0.2, a = 1 m, B = 3 T, q(o) = 1, A = 3.1 we obtain for ICRF-heating of ^{3}He ions: $T_* \cong 4.3$ MeV. Finally, fig. 3 illustrates the degradation of the fast ion energy content with increasing orbit width as characterized by the on-axis tail temperature, $T_\perp(0)$.

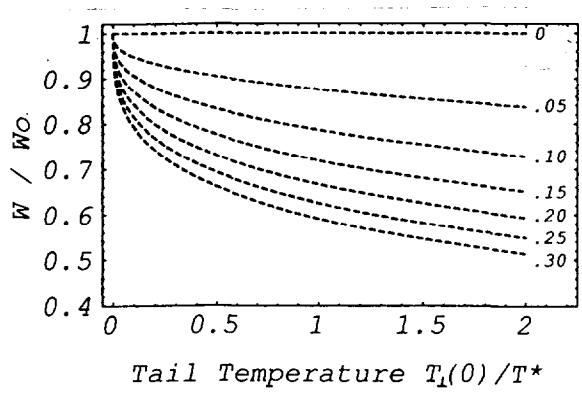

Fig. 3. Plot of the degradation of fast ion energy content with increasing orbit width as characterized by the normalized on-axis tail temperature $T_\perp(0)/T_*$ for different values of the parameter μb^2.

IV. SAWTOOTH-INDUCED REDISTRIBUTION OF ICRF HEATED PARTICLES

Experimental evidence indicates that sawtooth crashes tend to redistribute ICRF-heated particles, [1, 2]. In particular, the rapid reduction of the fast ion energy content following a sawtooth crash which has been observed on JET, was investigated by numerical simulations in [1]. The analysis was based on the assumption that the change in fast ion energy is due to the slowing down of fast ions that have been expelled from the central plasma to outside the q=1 surface. The short slowing down time experienced by the fast ions in the outer cooler parts rapidly reduces the energy of the high energy ions. For the analyzed discharge it was found that the drop in fast ion energy content was consistent with a scenario where only 60% of the fast ion energy remained inside the q=1 surface after the crash. This result was obtained by a trial procedure where a certain fraction, α, of the fast ion energy was transferred from inside the q=1 surface to the outside. By varying α and comparing the simulation results with experiments, the proper value of α could be determined. The inclusion of finite orbit effects was a crucial feature in the comparison.

In the present work we will use a recently presented model for predicting the redistribution of fast ions at sawtooth crashes, [6]. This model is a "smoothed" version of a more detailed theory for sawtooth induced redistribution of fast ions presented in [7]. The smoothed version should be useful when analyzing averaged quantities or when comparing with experimental results obtained with limited space and/or time resolution. This approximation should be applicable to the present problem involving the total integrated energy of the fast ions.

The model predicts that the precrash ion energy density profile

$$w(x) = w(0)\left(1 - x^2\right)^{\lambda} \tag{26}$$

after the crash becomes redistributed to

$$w_+(x) = w_+(0)\left(1 - x^2\right)^{\gamma_+} \tag{27}$$

where

$$\begin{aligned} w_+(0) &= w(0)\left(1 - x_s^2\right)^{\gamma} \\ \gamma_+ + 1 &= (\gamma + 1)\left(1 - x_s^2\right)^{\gamma} \end{aligned} \tag{28}$$

and x_s is the normalized radius of the q = 1 surface. We emphasize that as the simplified model indicates, the two most important parameters determining the redistribution is the peaking factor before the crash (γ) and the location of the q = 1 surface (x_s). The third important parameter is the ratio of the slowing down time to the sawtooth period which in the presently used formulation of the theory is assumed small.

The redistribution of the fast ion energy density according to the smoothed profile given by eqs. (26-28) is based on the assumption that the sawtooth crash conserves the total fast ion energy. This cannot be expected to be the case for very peaked density profiles in combination with large values of x_s where the corresponding mixing radius x_m, becomes comparable to the plasma radius. Thus, the approximate redistribution model should not be used for too large values of x_s; in the present application we will require $x_s < 0.4$.

Using eqs. (26-28) we find that the ratio, K, of the fast ion energy within the q = 1 surface after the crash as compared to the corresponding energy before the crash is given by

$$K \equiv \frac{\int_0^{x_s} w+(x)x\,dx}{\int_0^{x_s} w(x)x\,dx} = \frac{1 - \left(1 - x_s^2\right)^{\gamma_+ + 1}}{1 - \left(1 - x_s^2\right)^{\gamma + 1}} \tag{29}$$

We emphasize that this fraction is determined only by the location of the q = 1 surface and the peaking factor γ of the fast ion energy density profile. The dependence of K on x_s for different precrash peaking factors, γ, is illustrated in Fig. 4.

We now turn to an application to the discharge investigated in [1] (# 19650). The power deposition here is peaked off axis. To model this we use $b \approx 0.35$ which is slightly larger than the actual width of the profile itself ($b \cong 0.20$) but accounts for the off-axis location of theresonance surface cf [5]. Finite orbit effects can be estimated to give $\delta_{eff} \cong 0.12$ implying that the effective width of the power deposition profile is $b + \delta_{eff} \cong 0.47$. For the exponent of the slowing down profile we have $\mu \cong 3.1$. Consequently the peaking factor of the fast ion

energy profile is obtained as $\gamma \cong 7$ corresponding to an effective Gaussian width of 0.36 in fair agreement with the simulation results in [1] (cf. Fig.11). The q = 1 surface as inferred from the temperature inversion radius and the safety factor profile from the equilibrium code IDENTC [8] is approximately $x_s \cong 0.32$. Finally using eq. (29) we obtain $K \cong 0.59$ in agreement with the simulation results. A similar analysis has been made of several other pulses and theresult is summarized in Table II. The redistribution factor K is found to be of the order of 40-60 %.

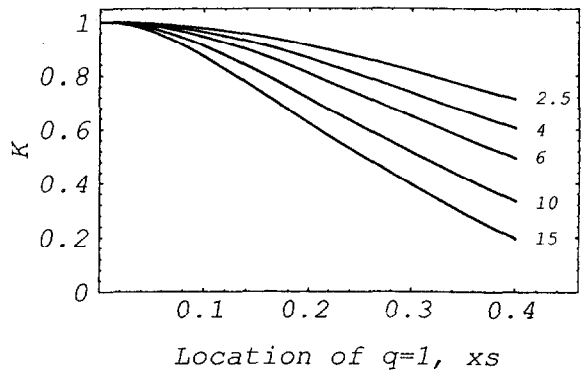

Fig. 4. Plot of the ratio, K, of total fast ion energy inside the q = 1 surface after the crash to the corresponding energy before the crash as a function of the location of the q = 1 surface and for different precrash fast ion energy peaking factors, γ.

Table II

pulse	W	γ_{eff}	x_s	K	w(0)	$w_+(0)$	$w_+(0)$ exp
19650	1.0	7	0.32	0.59	$1.3 \cdot 10^2$	61	60
15374	0.8	13	0.32	0.40	$1.9 \cdot 10^2$	47	50
15380	0.8	11	0.34	0.41	$1.6 \cdot 10^2$	41	43
15433	0.6	7	0.40	0.44	$0.8 \cdot 10^2$	23	21

Table II. Sawtooth induced redistribution of fast ion energy within the q = 1 surface as expressed by the parameter K, cf eq (29). The table also contains a comparison between the post crash on-axis fast ion energy density, as predicted by the redistribution model, $w_+(0)$, and the experimentally inferred value $w_+(0)_{exp}$ (except for #19650 which is a simulation result). The quantities W and w(0), $w_+(0)$, and $w_+(0)_{exp}$ are given in units of MJ and kJ/m^3 respectively.

If the central net heating rate of the electron energy density after a sawtooth crash, $dw_e^+(0)/dt$, is dominated by the slowing down of fast ions, the central energy density of the fast ions after the crash can be inferred from the experimentally determined electron reheating according to $w_+(0) \cong \left(t_s^+(0)/2\right) dw_e^+(0)/dt$, cf [2]. In Table II we also show a comparison between the experimentally inferred value of $w_+(0)$ and the theoretical predictions as obtained from eq. (29). The agreement is found to be good.

V. SAWTOOTH INDUCED CHANGE OF TOTAL FAST ION ENERGY

Finally we proceed to a qualitative discussion of the decay of the fast ion energy content after a sawtooth crash. The time variation of the total fast ion energy is determined by eq. (20). Assuming steady-state conditions before the crash, the total fast ion energy, W , is determined by eq. (21), i.e.

$$W = \frac{1}{2}\bar{t}_s P \tag{30}$$

At the crash, P remains constant. Furthermore, W has been assumed to be constant during the redistribution occurring on the crash time scale. However, due to the effectively shorter slowing down time caused by bulk plasma redistribution at the crash together with the sawtooth-induced broadening of the fast ion profile, W will decrease before it starts to recover to reach the steady-state value.

The post crash fast ion energy evolves according to

$$\frac{dW_+}{dt} = P_+ - \frac{2W_+}{\bar{t}_s^+} \tag{31}$$

with $\bar{t}_s^+ \equiv t_s^+(0)\frac{\gamma_+ + 1 - \mu_+}{\gamma_+ + 1}$ and

$$\bar{t}_s^+ \equiv t_s^+(0)\frac{\gamma_+ + 1 - \mu_+}{\gamma_+ + 1} \tag{32}$$

where μ_+ is the peaking factor of the post crash slowing down time profile $t_s^+(x)$.

The details of the time evolution of the drop and subsequent recovery of the fast ion energy would require an elaborate modelling of the recovery of $\bar{t}_s^+$. Nevertheless, it is instructive to estimate an upper bound on the drop of fast ion energy by assuming $\bar{t}_s^+$ to remain constant and determined by the corresponding sawtooth induced redistribution of electron particle and energy densities. This implies, cf eq (31)

$$\min\ W_+ \geq \frac{1}{2}\bar{t}_s^+ P_+ \equiv \Lambda W \tag{33}$$

where the energy degradation factor Λ is given by

$$\Lambda \equiv \frac{1}{2}\frac{\bar{t}_s^+}{W} = \frac{\gamma + 1}{\gamma_+ + 1} \cdot \frac{\gamma_+ + 1 - \mu_+}{\gamma + 1 - \mu}\left(1 - x_s^2\right)^{\mu} \tag{34}$$

However, the decay time for the drop in total fast ion energy, $\bar{t}_s^+ / 2$, is of the same order of magnitude as the characteristic time on which the bulk plasma recovers from the sawtooth

crash, i.e. the time scale for the recovery of $\bar{t}_s^+$ (e.g. $\bar{t}_s^+ / 2 < 0.1$s for discharge #19650). Consequently, the the drop in total fast ion energy, Λ, as given by eq. (34), tends to overestimate the drop in total fast ion energy, a feature which is reflected in the comparison between predicted and experimental drops given in Table III.

Table III

pulse	p	m	μ	γ_{eff}	x_s	Λ	Λ_{exp}
19650	0.65	2.5	3.1	7	0.32	0.7	0.8
15374	0.65	2.9	3.7	13	0.32	0.4	0.8
15380	0.50	2.0	2.5	11	0.34	0.5	0.7
15433	0.50	2.1	2.7	7	0.40	0.5	0.5

Table III. Sawtooth induced loss of total fast ion energy. A comparison between the predicted maximum possible energy drops and experimentally observed drops.

We also note that for very peaked fast ion energy density profiles combined with rather flat slowing down profiles ($\gamma >> \mu$), eq. (34) predicts a drop in total fast ion energy. However, in the opposite case of $\gamma < \mu$, eq. (34) actually predicts an increase in the total stored energy following a sawtooth crash. In this situation the strongly increasing slowing down time in the non-central plasma at the sawtooth crash combined with little redistribution of the fast ion energy profile should give rise to a rapid heating of the ions, thus boosting the total energy. The dependence of Λ on x_s as well as the importance of the relative magnitude of γ and μ is illustrated in Fig.5.

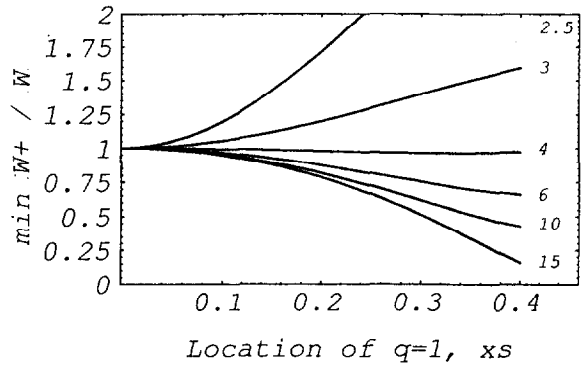

Fig. 5. Plot of the energy degradation factor Λ, as a function of the location of the $q = 1$ surface, x_s, and for different peaking factors, γ, of the precrash energy profile. The peaking factor of the slowing down profile is $\mu = 3.1$.

VI. CONCLUSION AND DISCUSSION

The present work has investigated sawtooth-induced redistribution of ICRF-heated minority ions in Tokamak plasma. An important prerequisite of the analysis has been to describe the profile broadening effect caused by the large orbit excursions from the magnetic surfaces of the high energy RF-heated minority ions. A model has been suggested which replaces the zero

orbit width fast ion profiles with profiles that are broadened by a suitable average of the orbit width. The accuracy of the simplified model is demonstrated by direct comparison with numerical simulation results and with measurements of the total fast ion energy content. Using the orbit broadened profiles a recently given model for sawtooth-induced fast ion redistribution is then applied to evaluate the on-axis fast ion energy density, the total fast ion energy content remaining within the q = 1 surface after the crash, and the drop in total fast ion energy content as the expelled fast ions rapidly slow down in the outer colder parts of the plasma. Comparison with numerical simulations and experimental results shows good agreement. In the analysis it has been assumed that the slowing down time of the ions is much less than the sawtooth period. In the opposite limit the minority ions will experience a strong radial mixing due to the sawteeth. Consequently the radial profiles of the fast ion energy density and the collisionally transferred power to the electrons can be expected to be almost flat within the mixing radius.

REFERENCES

[1] L.-G. Eriksson, T Hellsten, and U Willén, Nucl. Fus. **33** (1993), 1037.

[2] L.-G. Eriksson et al, Nucl. Fus. **29** (1989), 87.

[3] G A Cotrell and D F H Start, Nucl. Fus. **31** (1991), 61.

[4] L.-G Eriksson and F Porcelli, JET Report JETR (91) 11 (1991).

[5] J Jacquinot, G J Sadler, and the JET Team, Fusion Technology **21** (1992) 2254.

[6] D Anderson, P Batistoni, M Lisak, and F Wising, Plasma Phys. Control Fusion **35** (1993), 733.

[7] D Anderson , Ya I Kolesnichenko, M. Lisak, F. Wising, and Yu. V. Yakovenko, Nucl. Fusion **34** (1994), 217.

[8] M Brusati, J P Christiansen, J G Cordey, K Jarret, E Lazzaro, R T Ross, Comp. Phys. Rep. 1 (1984) 345 (IDENTC is an updated version of IDENTB described in this reference).